Out-of-Plane Soft Lithography for Soft Pneumatic Microactuators Arrays

Edoardo Milana,[1] Benjamin Gorissen, [1] Eline De Borre,[1] Frederik Ceyssens,[2] Dominiek Reynaerts,[1] and Michael De Volder[1,3,]*

* corresponding author

1. Department of Mechanical Engineering, KU Leuven and Flanders Make, Leuven, Belgium.
2. Department of Electrical Engineering (ESAT), KU Leuven, Leuven, Belgium.
3. Institute for Manufacturing, Department of engineering, University of Cambridge, Cambridge, UK.

Keywords: soft lithography, soft bending microactuators, artificial cilia, active pillars, soft robotics

Abstract:

Elastic pneumatic actuators are fuelling new devices and applications in soft robotics. Actuator miniaturisation is critical to enable soft microsystems for applications in microfluidics and micromanipulation. This work proposes a fabrication technique to make out-of-plane bending microactuators entirely by soft lithography. The only bonding step required is to seal the embedded fluidic channels, assuring the structural integrity of the microactuators. The process consists of fabricating two SU8 mold halves using different lithographic layers. Polydimethilsiloxane (PDMS) is poured on the bottom mold, which is subsequently aligned and assembled with the top mould. The process allows for out-of-plane actuators with a diameter of 300 μm and for fabricating arrays of up to 36 actuators that are row-addressable. These active micropillars have an aspect ratio of 1:1.5 and when pressurized at 1 bar, show a bending angle of approximately 30°.

1. Introduction

Flexible actuators are a key technology for the development of new microscale systems that mimic active biological tissues. In addition, soft actuators have the advantage that they typically do not have joints and therefore they do not suffer from friction and phenomena such as stick-slip [1]. As a result, they are attractive for bio-MEMS, minimally invasive surgery, microfluidics and microrobotics [2]. In this work we seek to develop arrays of soft flexible microactuators. More specifically, we are studying flexible active micropillar arrays, which may be adopted in the future as micromixing and micropumping devices [3] by mimicking biological cilia [4-9] .

To date, most artificial cilia consist of micropillars that are made out of a composite material consisting of an elastomeric matrix with magnetic micro or nanoparticles as a filler for actuation using a magnetic field [10-14]. While impressive, a limitation in these flexible magnetic actuators is that they are controlled by an external magnetic field, which limits the local control of the cilia motion. The latter is important to achieve symmetry breaking in the motion of the cilia, which is crucial to create propulsion in low Reynolds number regimes.

Recently, our research group has shown that these issues can be alleviated by changing actuation principles and using out-of plane soft inflatable bending actuators [15,16]. Inflatable soft actuators rely on a pressurised fluid (typically air) to inflate an elastic structure and hence generate motion. These soft pneumatic actuators can be designed to generate different types of deformation such as extension, contraction, bending and twisting [17]. The bending motion of these actuators is created by pressurizing a cavity that is placed eccentrically with respect to the longitudinal axis, resulting in a bending motion towards the stiffest part of the cross section.

Initially, small-scale pneumatic bending actuators were fabricated by bonding two PDMS sheets processed using soft-lithography 2D micromolding [18]. However, this design can suffer from delamination issues between the bonded layers as well as a large dimensional variability due to manual cutting steps that are required. An alternative approach for fabricating these

devices is using a 3D mold that alleviates the need for bonding different layers and for manually cutting [19–21]. However, the fabrication of the 3D molds using classic manufacturing processes (micromilling and microdrilling) results in actuators that can have outer diameters down to 1 mm and is a limit to further downscaling. Moreover, this production process makes it difficult to fabricate actuators in large arrays, due to the manual assembly of the moulds. To avoid these assembly challenges in small-scale inflatable actuators, a laser cutting process has been proposed using sheets of thermoplastic polyurethane [22] as well as a process using a combination of lithography and dry etching of PDMS [23]. These techniques allows for a rapid manufacturing of small actuators but cannot be used for direct fabrication of 3D out of plane actuators.

This work explores a new approach for fabricating 3D small-scale soft actuators with all dimensions in the sub-millimeter range by using lithographically fabricated micromolds. This enables to further decrease the actuator dimensions and to address the challenges in fabricating actuator arrays using the processes described above. Compared to similar moulding processes described previously, the lithographic micromolding process developed in this work allows reducing the diameter of these actuators by more than 3-fold, and arrays of 36 actuators are fabricated in one step, which is an important improvement over current piece-wise fabrication methods.

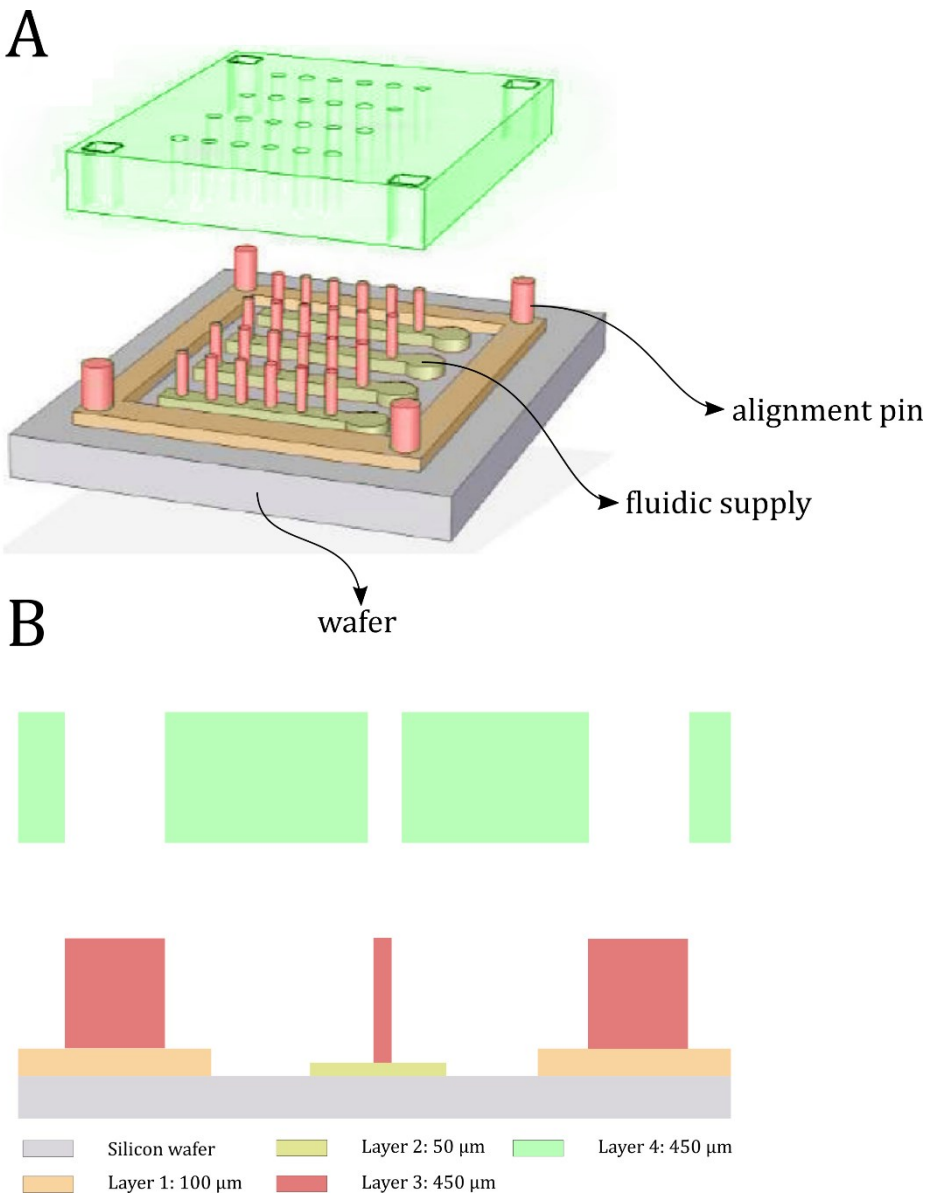

[Figure 1. A. 3D representation of the two halves of the micromould. B. Section view of the mould. Colour codes are consistent in all following figures and identify the different layers produced with the lithography process: orange is *Layer 1*, yellow green is *Layer 2* and light red *Layer 3* of the bottom mould, and light green is the top mould.]

2. Materials and Methods

2.1 Mould design

The lithographically developed moulds in this work consist of two parts (top and bottom mould) as depicted in Figure 1. The bottom mould consists of a multiple-layered SU8 structure on a Si wafer. The top part is a free standing SU8 structure consisting of a single layer.

The bottom mould consists of three lithographical layers, all with a different height (see Figure 1) thus requiring the design of three photomasks. The first layer forms the rectangular outside walls of the mould that are 100 µm thick. The thickness of the walls defines the vertical position of the top mould and therefore the thickness of the base of the microactuators. The second layer is 50 µm thick, shown in yellow in Figure 1 and defines the fluidic channels that connect the microactuators' internal voids to the pressure supply. The connection with external tubing is made by punching a hole in a circular feature (2 mm in diameter) with a biopsy punch and inserting a tube. The last layer of the bottom mould (light red in Figure 1) defines the 450 µm long pillars corresponding to the inner cavity of the actuator that are placed on top of the fluidic channels. The radius of the pillars (r) is 90 µm. Moreover, this third layer defines the alignment pins located at the four corners of the outside wall. Those alignment pins are 400 µm in length and 500 µm in diameter, and their function is to align both halves of the mould.

The top mould is a rectangular SU8 plate that is 450 µm thick, which corresponds to the height of the microactuators, with through holes defining the outside diameter of the microactuators. The radius of the holes (R) is 150 µm. The microactuators have an aspect ratio (AR) of 1:1.5. Additional 510 µm diameter through holes are designed to fit the alignment pins. As can be seen on Figure 1B, the alignment pins are vital to ensure an accurate eccentric placement of the pillars of the bottom part of the mold with respect to the cylindrical voids defined in the top

part of the mould. This eccentricity (e) is 42 µm in our design. As the space between the pillar and the holes of the top moulds defines the smallest feature of the microactuators, corresponding to t=R-r-e=18 µm, mould alignment is a critical step. The larger nominal dimension of the alignment holes imposes a nominal clearance of 10 µm, which would still guarantee the mechanical assembling of the two moulds and compensate for the SU8 process tolerances[24]. Smaller designs (r = 30 µm, R = 50 µm, AR = 1:4.5) are also included in the photomasks, even if the 10 µm clearance might lead to mechanical incompatibility.

Figure S1 in Supplemental Information depicts the superimposition of the three photomasks used for the bottom mold process. The third inset depicts also the detail of the superimposition of the top mold photomask (dark green) on top of the actuator structure, showing the eccentricity between the top mold hole and the bottom mold pillar.

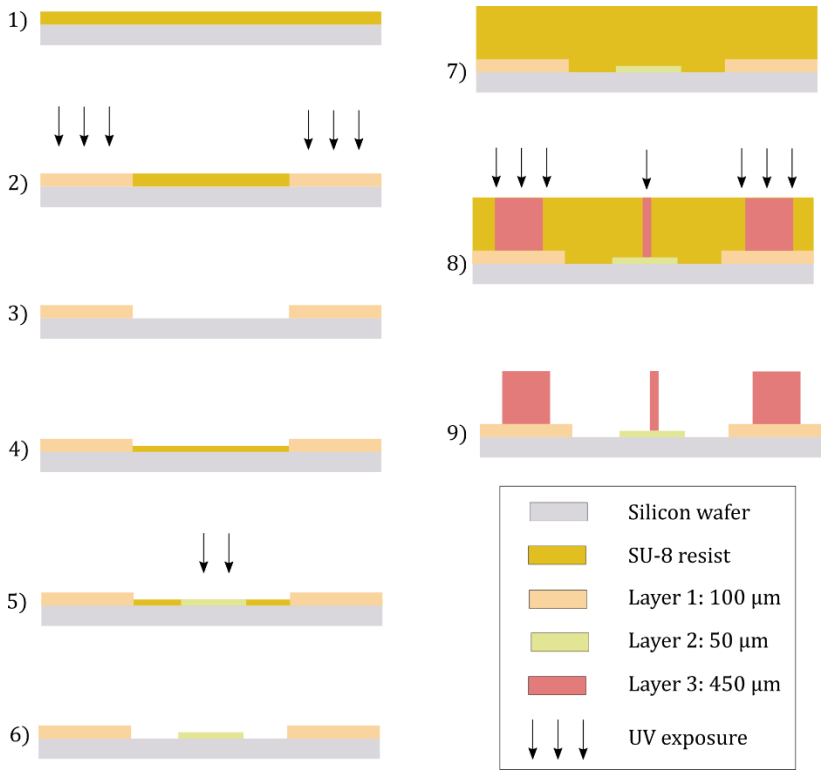

[Figure 2. Process steps for fabricating the bottom mold using SU8 lithography.]

Previously reported actuators casted in micromilled moulds [19,20] have thicknesses of the thinnest section of t=40 µm. Therefore, controlling the position of the top mold accurately relative to the bottom mold is extremely important to avoid variations in the cross-section geometry that strongly affects the bending motion.

2.2 Lithographic mould fabrication

As described above, the bottom mould consists of three layers that can be fabricated using the lithography process depicted in Figure 2. *Layer 1* (100 µm thick) is fabricated by spin-coating SU-8 2100 (MicroChem) for 30 s at 3000 rpm on a 4-inch silicon wafer. The wafer is soft baked for 5 min at 65 °C and then 30 min at 95 °C. An i-line filter is used during the UV exposure (dose 250 mJ cm^2). Post exposure bake is done for 1 hour at 80 °C and, subsequently, the wafer is developed in PGMEA.

Layer 2 (50 µm thick) is made using SU8 2050 (MicroChem), spin-coated for 30 s at 3000 rpm. The layer is soft baked for 1 hour at 65 °C and exposed using an i-line filter (dose of mJ cm^2). Post exposure baking is carried out at 80 °C for 1 hour. After cooling down, the wafer is developed in PGMEA.

The third layer of the bottom mold (*Layer 3*), featuring the 450 µm long pillars, is made by casting 6.76 g of SU-8 with a solvent concentration of 47.5%, on the wafer. For these thick layers, we obtained better results using casting rather than spin coating, following a previous report[25]. The mass of the drop-casted SU8 is calculated based on the surface area of the wafer, the desired height and the volume of the two SU-8 layers already developed. The SU-8 used in this process is obtained by diluting SU-8 2150 (MicroChem) (24.25% solvent concentration) with the solvent SU-8 2000 thinner (MicroChem), in order to decrease its viscosity and achieve a uniform photoresist spread. The soft bake step is done at 75 °C, while the weight of the wafer is periodically measured on a scale to monitor the solvent evaporation. The process proceeds until the solvent concentration decreases to 5.2%. This optimal value is found after a process

characterization, where several *Layer 3* patterns were developed with different solvent concentrations ranging from 2.7% to 7.4%. Concentrations lower than the optimal value resulted in the collapse of the pillars probably due to higher internal stresses caused by the cross-linking. On the other hand, higher concentrations resulted in bent pillars. A PMMA filter and a dosage of 12 mJ cm^2 are used during the UV-exposure. The post exposure bake is done for 1 hour at 80 °C and the SU-8 is developed in PGMEA.

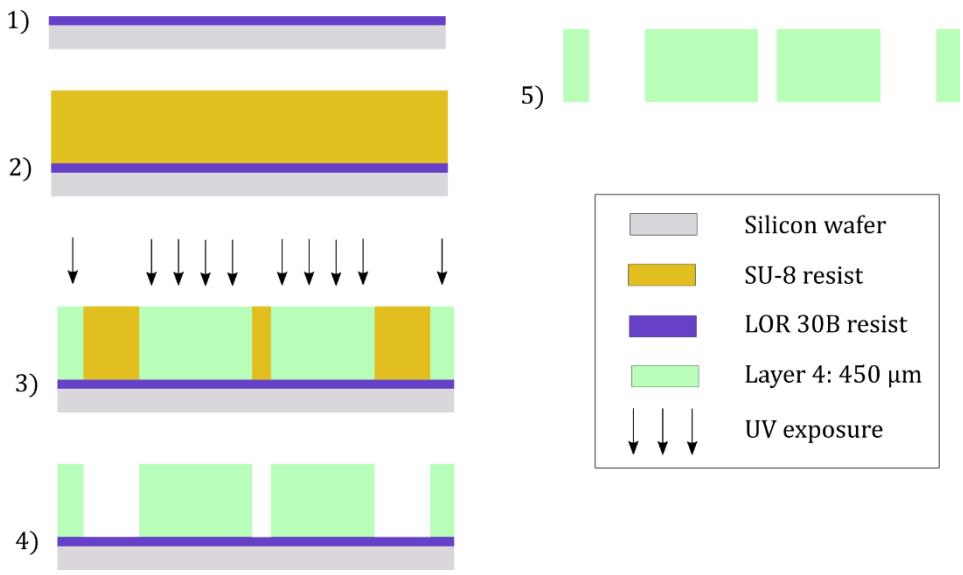

[Figure 3. Process steps for fabricating the top mold using SU8 lithography.]

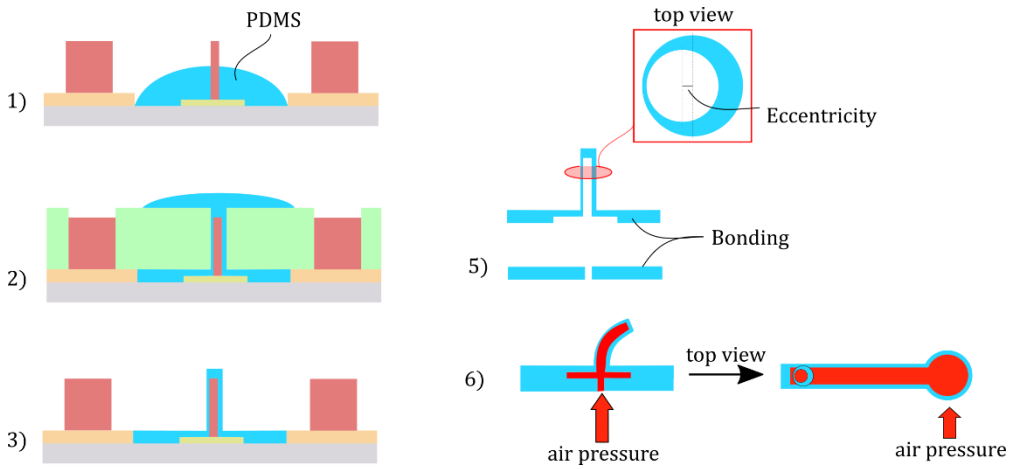

[Figure 4. PDMS microactuator casting and bonding process.]

The manufacturing process of the top mold is analogous to the one of the third layer of the bottom mold (Figure 3). However, since the top mold is a free-standing piece to be manipulated and aligned to the bottom mold, a sacrificial layer is added to the process to remove the SU8 layer from the wafer. This sacrificial layer is a 3 µm thick LOR 30B (MicroChem) resist, spin-coated on a 4-inch silicon wafer at 2000 rpm for 30 s. The wafer is subsequently backed for 5 min at 170 °C. 6.58 g of SU-8 (see above) is then cast on top of the LOR30B to form a 450 µm thick layer. The soft bake step is done at 75 °C until 5.2% solvent concentration is achieved. UV-exposure is done with a PMMA filter and a dosage of 12 mJ cm^2. Post exposure bake is done for 1 hour at 80 °C and the SU-8 is developed in PGMEA. After development, the sacrificial layer is removed by placing the wafer in 351 Developer (Microposit) overnight.

2.3 PDMS casting and assembling.

To create an array of bending actuators, the process illustrated in Figure 4 is followed. first, PDMS prepolymers (Sylgard 184, DOWSIL) are mixed in a ratio 1:10 and degassed in a vacuum chamber for 5 min. The bottom mold is placed under an optical microscope and the PDMS blend is poured on the bottom mold in the area delimited by the external wall shown in Figure 4.1).

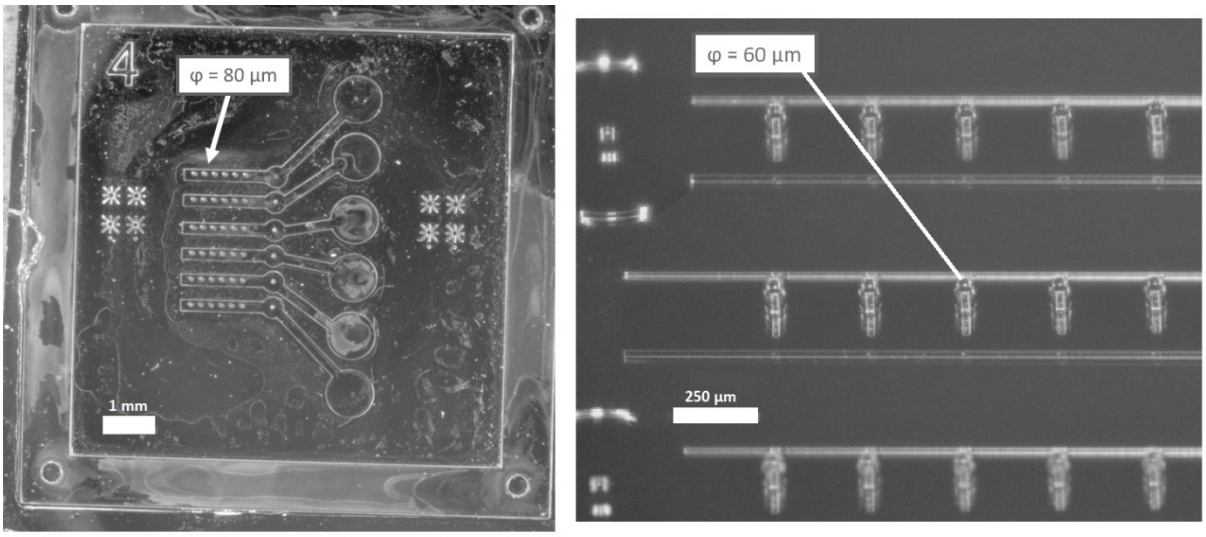

[Figure 5. Bottom molds optical microscopy images. Pillar diameters are reported in the insets.]

The top mold is then placed on top of the PDMS meniscus. As the top layer floats on the liquid PDMS, it can be manipulated with tweezers to align the positioning holes and pins under the microscope. Then, the two molds are pushed in contact, squeezing out the excess of PDMS from the mold. A weight is applied to hold the two parts together. PDMS curing times are substantially affected by temperature [26]. However, temperature increase tends to deform the top mold, therefore PDMS curing is done at room temperature for approximately 48 hours. Afterwards, the moulded structures are carefully released using ethanol. First, the top mold is removed carefully not to break the brittle SU-8 layer. Next the PDMS layer can be easily peeled off the bottom mold. The demoulded PDMS layer then needs to be bonded to a flat PDMS substrate, to seal the fluidic channels and to provide fluidic connections. For the flat PDMS layer, a 5 mm thick substrate is cast and 1 mm diameter holes are punched in this layer using a biopsy punch to connect external fluid supplies to the circular cavity shown in the top view inset of Figure 4. The PDMS substrate and microactuators layer are then activated in a plasma cleaner (oxygen plasma 200 mTorr for 30 s) to enable the bonding. The two layers are aligned such that the holes punched in the substrate are aligned with the correspondent supply channels in the moulded PDMS layer. To strengthen the bond, the PDMS is baked for 24 h at 60 °C. Lastly, a 1 mm outer diameter tube is inserted in the hole and glued to the substrate with uncured PDMS. The tube is then connected to a pressure source.

3. Results

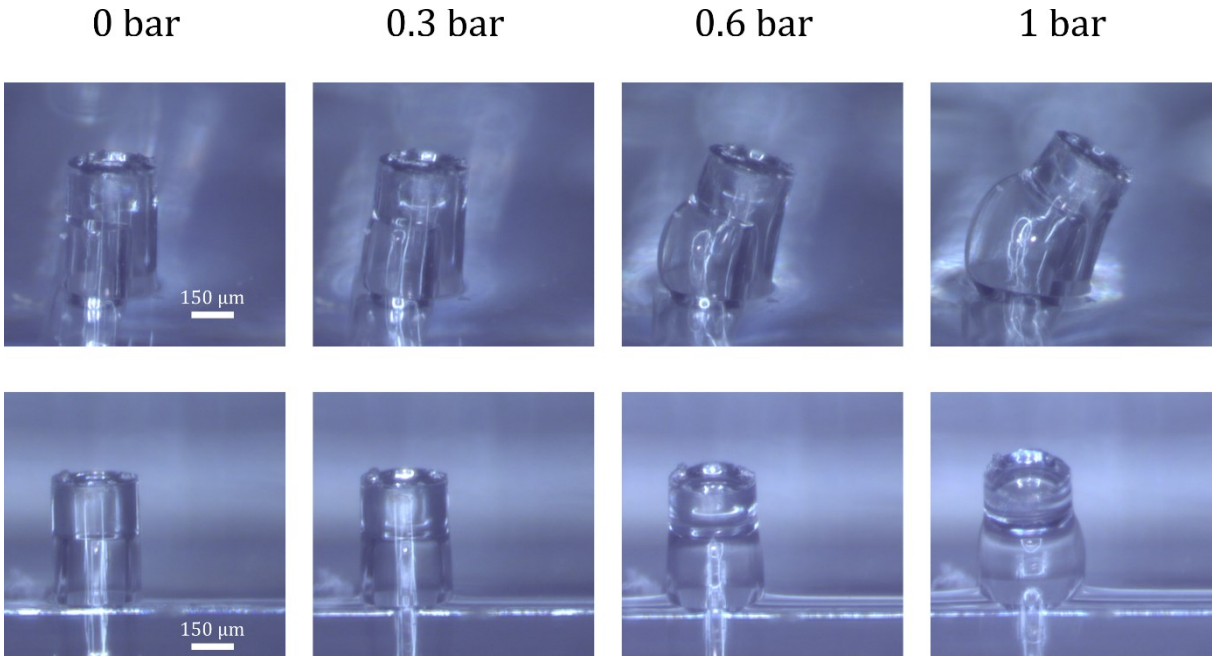

[Figure 6. Lateral and front view of a micropillar (R=150, r=90, e=42 µm) inflation at 0, 0.3, 0.6, 1 bar.]

Optical microscopy images of the bottom half of the mould are provided in Figure 5. To understand the actuator properties and their fabrication limitations, several actuator geometries were designed on the photomasks. As anticipated in the previous section, smaller actuator design with AR values of 1:4.5 could not be fabricated using our process due to limitations in the mould alignment accuracy. Moreover, since the top mould is a free-standing SU-8 layer, cracks easily form as a consequence of internal stresses caused by the solvent evaporation (Figure S2A). Further, not all the small holes (R = 50 µm) were fully developed through the layer (Figure S2B). The main issue related to internal stresses, is that the SU-8 layer tends to bend, especially when heated up. This limits the PDMS curing temperature as discussed above. In addition, the curvature of the top layer can also prevent the mold from begin fully closed (Figure S2C), resulting in the failure of the casting process or a mismatch in the actuator dimensions. In fact, due to the gap between the two halves of the mould, the pillars could only

partially enter in the top mould, resulting in actuators with shorter inflatable cavities and longer tips (Figure S3). Those actuators exhibit no significant deformation when inflated. Indeed, for the bending moment to be distributed through the whole structure and, therefore, to have a substantial curvature of the actuator, the cavity needs to extend through the axial direction.

However, actuators with AR = 1:1.5 were successfully fabricated and tested using optical microscopy to visualize and measure the bending deformation. Figures of arrays of bending actuators are provided in Supplemental information (Figure S4). The figures show details of the array structure of the actuators and of the eccentricity of the inflatable cavity. Those images are taken before the bonding step that encloses the fluidic channels. After the fluidic connection is provided, as described in the Materials and Methods section, the actuators are inflated. Figure 6 shows the lateral and frontal view of the bending deformation of a pillar with the following dimensions: R=150 µm, r=90 µm and e=42 µm. The pillars are pneumatically inflated in a step-wise manner (0.1 bar per step, here 0.3, 0.6 and 1 bar are shown) to characterize the actuators in a quasi-static manner. The pillar progressively bends as the pressure is increased, as expected from observations made on large-scale inflatable actuators of the same type [19]. Despite the limited aspect ratio (1:1.5) and length of the actuators, their deflection is appreciable. The maximum bending angle is roughly 30° and the horizontal tip displacement is about 220 µm at a supply pressure of 1 bar. An analysis of the tip displacement as well as the bending angle as a function of the applied pressure is reported in Figure S5. These measurements illustrate that the moulding process for these pillars is sufficiently accurate to obtain the eccentricity of the inflatable cavity needed for actuation. Indeed, the images show the thin membrane inflating while the thick membrane tilts. From the frontal view, the substantial inflation and ballooning of the pillar is clearly observed. In order to analyse the experimental measurements, we compare them to finite element simulations (see details in SI). Figure 7 shows simulations of the actuator deflection, which are in good agreement with the experiments carried out at the same pressure

values in Figure 6. Next, we use this model to predict the blocking force of the microactuator, which is difficult to measure due to their small dimension. Our modelling results predict a blocking force of 1.8 mN in the vertical direction at 1 bar, in principle this force can be increased by applying higher pressure to the actuators, but in practice we found that at pressure of 1.1 to 1.2 bar, the microactuators fail due to the delamination of the two bonded PDMS layers, opening up the fluidic channels. Contrary to 2D planar microactuators where the delamination breaks apart the actuators, here the microactuators themselves do not burst and maintain their integrity. Therefore, we envision that future designs with better sealed supply channels will achieve higher forces.

Figure 8 shows a top view of an array of microactuators with the same size, where the inflated array (1 bar) is displaced compared to the neighbour deflated array. In order to estimate the deflection from this top-view an image analysis is conducted, considering the projected shapes of the pillars tip. The inflated shape of the tip is extracted from the image. Given the small curvature and short length, it can be assumed that the plane parallel to the tip is simply rotating around the axis of the pillars array. The tip projection is therefore rotated until it matched the tip projection of the deflated state. This image analysis confirms that 30° bending angle is an accurate measurement.

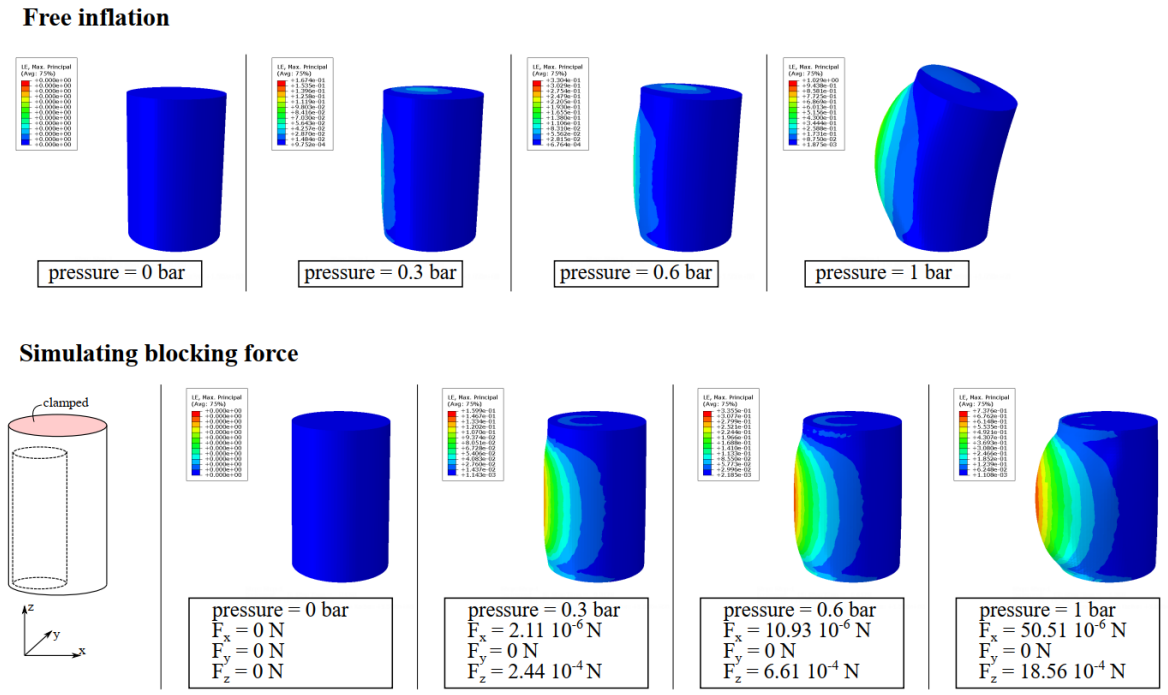

[Figure 7. FEM simulation of the microactuator. In the upper panel the free inflation is depicted at the same steps as Figure 6. In the bottom panel the blocking force simulation is reported at the same pressure steps]

Finally, we investigate the actuation frequencies of the developed actuators. The microactuators are functional in frequencies ranges comparable to the one of their larger-scale versions[15], up to a roughly 2 s per cycle. Higher frequencies result in negligible displacements of the microactuators likely due to the dynamic effects of the inflation process. A reason why the frequency response of these microactuators is not higher than large volumes is the large expansion of the thin membrane (Figure 6), requiring substantial time to inflate. This problem is typically solved for large-scale actuators by reducing the volumetric increase, either modifying the structure of the inner cavity with bellows or reinforcing the cavity with fibers. However, those strategies cannot be easily integrated with the process proposed here, making this an open challenge for future research on microfabrication of inflatable actuators.

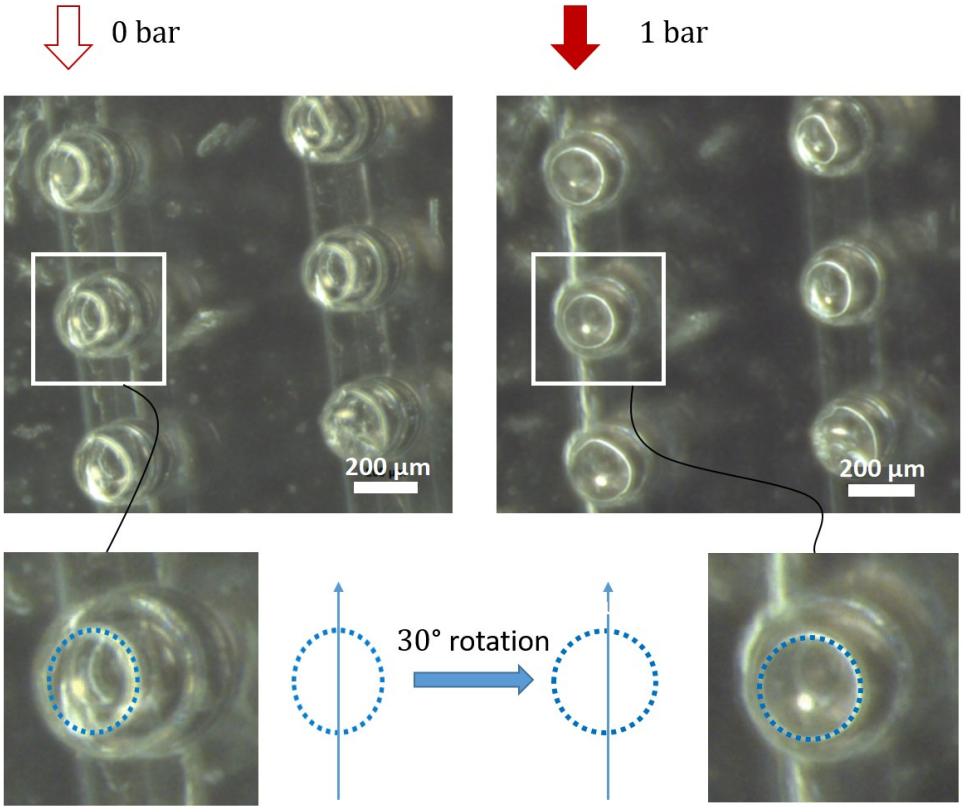

[Figure 8. Top view of an array of microactuators actuated at 1 bar. Image analysis of the tilted shape the tip coherent with a 30° angle.]

4. Conclusion

This paper reports a new fabrication processes for sub-millimeter sized soft inflatable actuators. This new process is relying on multi-layer SU-8 soft lithography to create 3D micromoulds. The moulds define both the actuators and the microfluidic channels for pressure supply. Several moulds are fabricated to cast actuators of different dimensions. Microactuators with membranes down to 18 µm and aspect ratios of 1.15 could be successfully manufactured and pressurized, showing a bending angle of approximately 30° at 1 bar. The microactuators developed in this work are three times smaller than the current state of the art, and in addition, arrays of 36 actuators were fabricated in one step, which is an important advantage of the previous piece-wise moulding process and paves the way to microengineering and microfluidic applications such as microciliary propulsion and micropillary manipulation. Further miniaturisation could

not be achieved with the current process and the smaller actuator designs with thinnest membrane of 3 μm and aspect ratios of 1:4.5 failed to be manufactured due to alignment issues and to the brittle SU8 top mould. Given that the top mould is the main limiting factor in the current design and that its geometry is relatively simple compared to the bottom mold, in future work it could be considered combining a lithographically fabricated bottom mould with a top mould fabricated by micromachining processes.

Acknowledgements

Funding: Research was supported by the Fund for Scientific Research-Flanders (FWO).

Author contributions: All authors contributed and revised the manuscript. **Data and materials availability:** All data used to generate the figures is available upon reasonable request.

Author Disclosure Statement

No competing financial interests exist.

References

1. De Volder M, Reynaerts D. Pneumatic and Hydraulic Microactuators: A Review. J. Micromechanics Microengineering. 2010;20(4):43001.
2. Hines L, Petersen K, Lum GZ, Sitti M. Soft Actuators for Small-Scale Robotics. Adv. Mater. 2017;29(13).
3. Pawinanto RE, Yunas J, Hashim AM. Design Optimization of Active Microfluidic Mixer Incorporating Micropillar on Flexible Membrane. Microsyst. Technol. 2019;25(4):1203–1209.
4. Toonder JMJ den, Onck PR. Microfluidic Manipulation with Artificial/Bioinspired Cilia. Trends Biotechnol. 2013;31(2):85–91.
5. Keißner A, Brücker C. Directional Fluid Transport along Artificial Ciliary Surfaces with Base-Layer Actuation of Counter-Rotating Orbital Beating Patterns. Soft Matter. 2012;8(19):5342.
6. Orbay S, Ozcelik A, Bachman H, Huang TJ. Acoustic Actuation of in Situ Fabricated Artificial Cilia. J. Micromechanics Microengineering. 2018;28(2):025012.
7. Hanasoge S, Ballard M, Hesketh PJ, Alexeev A. Asymmetric Motion of Magnetically Actuated Artificial Cilia. Lab Chip. 2017;17.
8. Wang Y, den Toonder J, Cardinaels R, Anderson P. A Continuous Roll-Pulling Approach for the Fabrication of Magnetic Artificial Cilia with Microfluidic Pumping Capability. Lab Chip. 2016;16(12):2277–2286.
9. Purcell EM. Life at Low Reynolds Number. Am. J. Phys. 1977;453–11.
10. Evans BA, Shields AR, Carroll RL, Washburn S, Falvo MR, Superfine R, Hill C, Hill C, Carolina N, Virginia W, *et al.* Magnetically Actuated Nanorod Arrays as Biomimetic Cilia. Nano Lett. 2007;7(5):1428–1434.
11. Vilfan M, Potocnik A, Kavcic B, Osterman N, Poberaj I, Vilfan A, Babic D. Self-Assembled Artificial Cilia. Proc. Natl. Acad. Sci. U. S. A. 2010;107(5):1844–1847.

12. Wang Y, Gao Y, Wyss H, Anderson P, den Toonder J. Out of the Cleanroom, Self-Assembled Magnetic Artificial Cilia. Lab Chip. 2013;13(17):3360–3366.
13. Zhang S, Wang Y, Lavrijsen R, Onck PR, den Toonder JMJ. Versatile Microfluidic Flow Generated by Moulded Magnetic Artificial Cilia. Sensors Actuators, B Chem. 2018;263614–624.
14. Hussong J, Schorr N, Belardi J, Prucker O, Rühe J, Westerweel J. Experimental Investigation of the Flow Induced by Artificial Cilia. Lab Chip. 2011;11(12):2017–2022.
15. Milana E, Gorissen B, Peerlinck S, De Volder M, Reynaerts D. Artificial Soft Cilia with Asymmetric Beating Patterns for Biomimetic Low-Reynolds-Number Fluid Propulsion. Adv. Funct. Mater. 2019.
16. Milana E, Zhang R, Vetrano MR, Peerlinck S, De Volder M, Onck PR, Reynaerts D, Gorissen B. Metachronal Patterns in Artificial Cilia for Low Reynolds Number Fluid Propulsion. Sci. Adv. 2020;6(49).
17. Gorissen B, Reynaerts D, Konishi S, Yoshida K, Kim J-W, De Volder M. Elastic Inflatable Actuators for Soft Robotic Applications. Adv. Mater. 2017;1604977.
18. Konishi S, Kawai F, Cusin P. Thin Flexible End-Effector Using Pneumatic Balloon Actuator. Sensors Actuators, A Phys. 2001;89(1–2):28–35.
19. Gorissen B, Vincentie W, Al-Bender F, Reynaerts D, De Volder M. Modeling and Bonding-Free Fabrication of Flexible Fluidic Microactuators with a Bending Motion. J. Micromech. Microeng. 2013;2345012–10.
20. Milana E, Bellotti M, Gorissen B, Qian J, De Volder M, Reynaerts D. Shaping Soft Robotic Microactuators by Wire Electrical Discharge Grinding. Micromachines. 2020.
21. Nagaoka T, Mao Z, Takemura K, Yokota S, Kim J. ECF (Electro-Conjugate Fluid) Finger with Bidirectional Motion and Its Application to a Flexible Hand. Smart Mater. Struct. 2019;28(2):25032.

22. Amiri Moghadam AA, Alaie S, Deb Nath S, Aghasizade Shaarbaf M, Min JK, Dunham S, Mosadegh B. Laser cutting as a rapid method for fabricating thin soft pneumatic actuators and robots. Soft robotics. 2018 28;5(4):443-51.

23. Gorissen B, Van Hoof C, Reynaerts D, De Volder M. SU8 etch mask for patterning PDMS and its application to flexible fluidic microactuators. Microsystems & nanoengineering. 2016 12;2(1):1-5.

24. Ceyssens F, Puers R. SU-8 Photoresist. In *Encyclopedia of Nanotechnology*; 2016.

25. Bogdanov AL, Peredkov SS. Use of SU-8 Photoresist for Very High Aspect Ratio x-Ray Lithography. Microelectron. Eng. 2000.

26. Johnston ID, McCluskey DK, Tan CKL, Tracey MC. Mechanical Characterization of Bulk Sylgard 184 for Microfluidics and Microengineering. J. Micromechanics Microengineering. 2014;24035017.

Address correspondence to:

Prof. Michael De Volder

Institute for Manufacturing - Department of Engineering

University of Cambridge

17 Charles Babbage Road

Cambridge, CB3 0FS

United Kingdom

E-mail: mfld2@cam.ac.uk

Supplemental Information

Out-of-Plane Soft Lithography for Soft Pneumatic Microactuators Arrays

Edoardo Milana, Benjamin Gorissen, Eline De Borre, Frederik Ceyssen, Dominiek Reynaerts, Michael De Volder

FEM Simulation

The FEM simulation is performed using the software Abaqus. We simulated the microactuator that is experimentally characterized, thus having the following dimensions: outer radius R=150 μm, inner radius r=90 μm, eccentricity e=42 μm, length L=450 μm and cavity length l=400 μm. PDMS is modelled as neo-hookean material with initial shear modulus of 0.424 MPa. The inflation is simulated using the general/static procedure. In figure S6 we report the results of two different simulations. Free Inflation, where the actuator is just clamped at the base and show a bending deformation, with the same configuration as the experimental characterization. Second, Blocking Force, where the actuator is clamped at both sides (base and tip) and the force exerted at the tip is computed in all three directions.

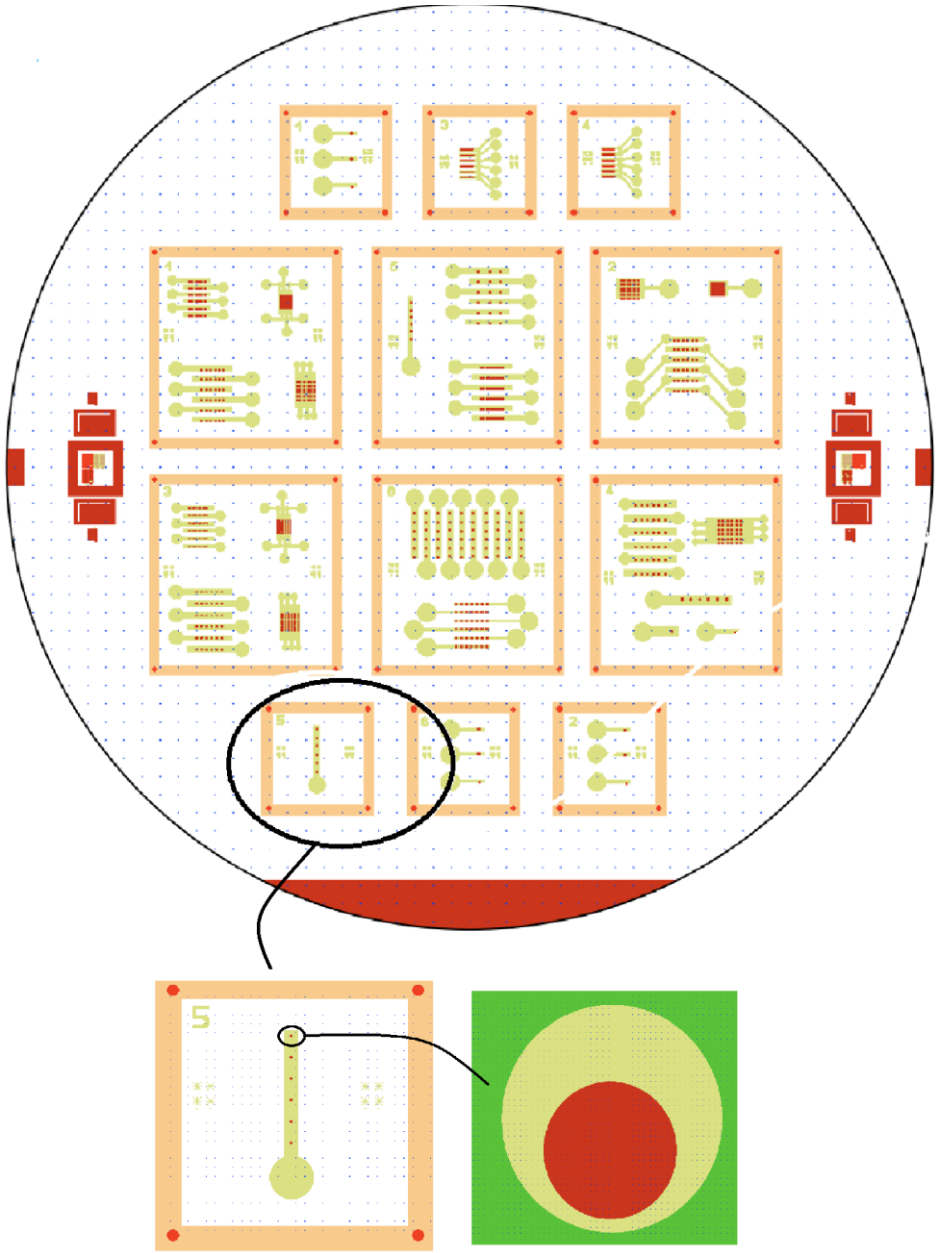

Figure S1. Three mask designs for the bottom moulds, each square is a mould as depicted in the insert. Details of the masks featuring the a micropillar, where light green is Layer 2 and red Layer 3 of the bottom mould, and dark green is the mask of the top mould (Layer 4)

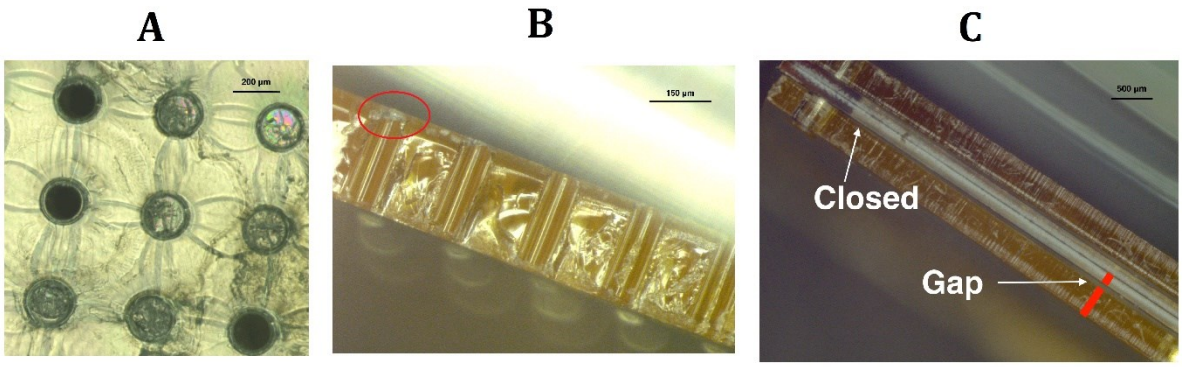

Figure S2. Top mould defects. A. Surface crack on the free-standing SU8 layer and not fully developed holes. B. Cross-section cut and particular of the obstructed hole. C. Detail of the gap between the two moulds caused by the bent deformation of the top mould.

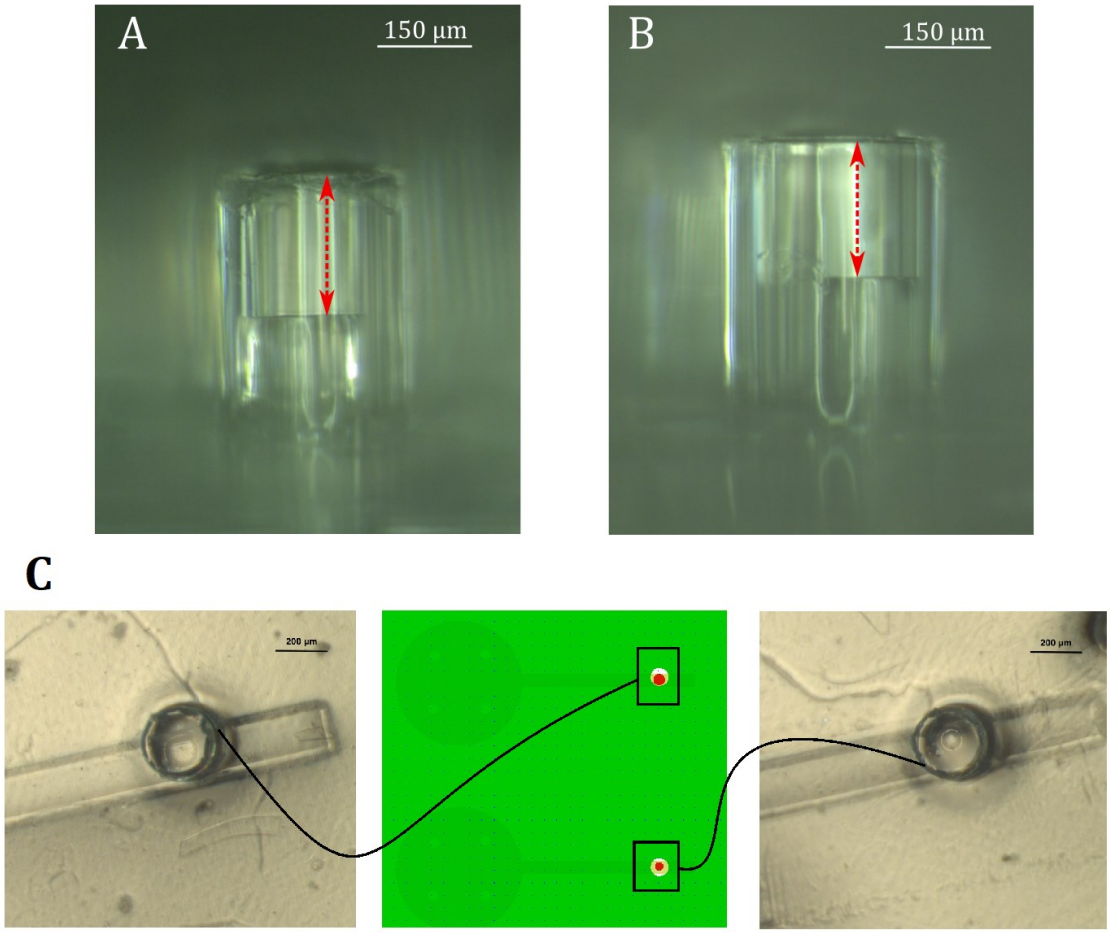

Figure S3. A and B. microactuators with defects. The inflatable cavity is not completely through the outer cylinder. The pillar tip should be 50 µm long, while the measured one is about 200 µm. C. Details of microactuators and comparison with the mask design.

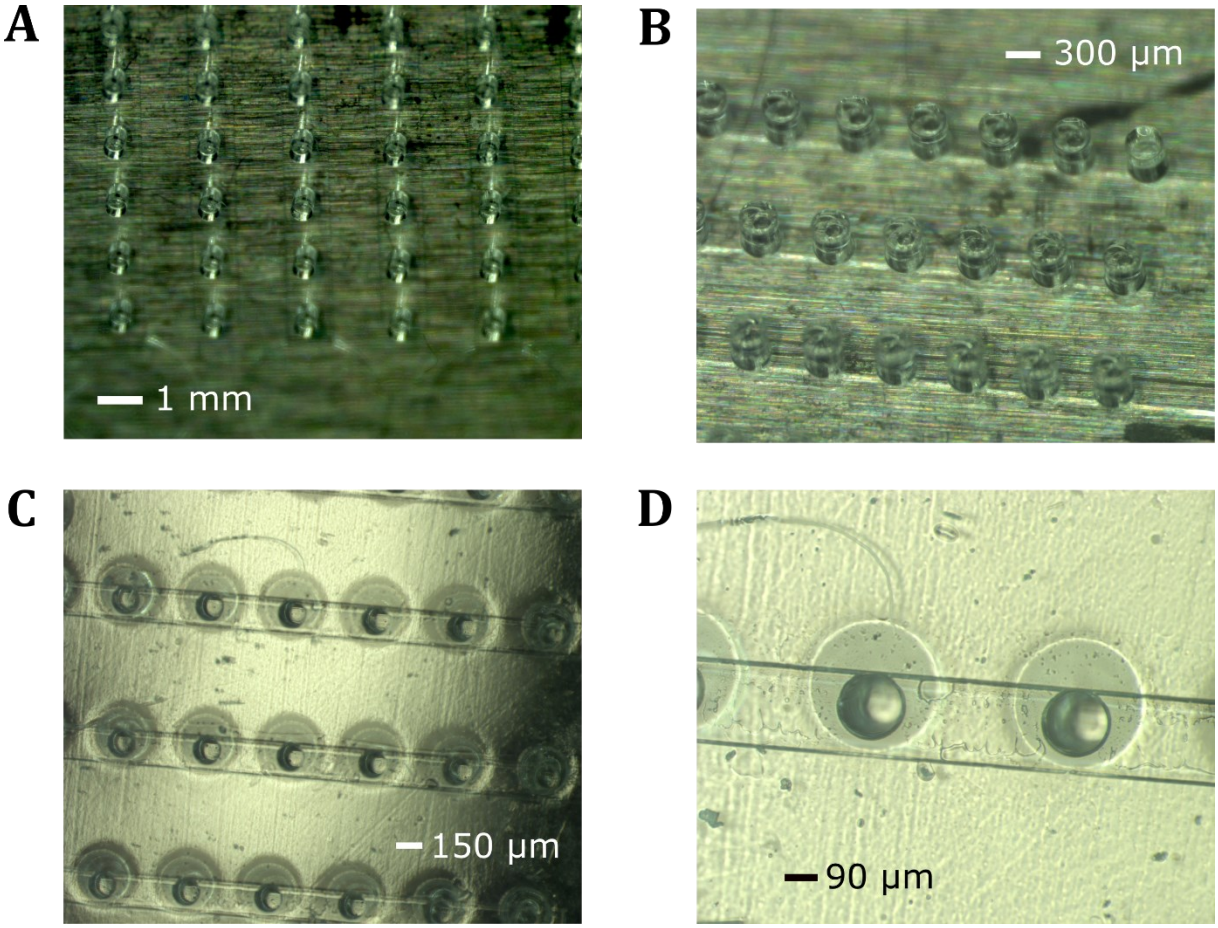

Figure S4. Array of microactuators details. A and B. Tilted view of the microactuators array with dimensions: L = 450 µm, R = 150 µm, r = 90 µm. C and D. Bottom view of the array with details on the eccentricity of the inflatable cavity.

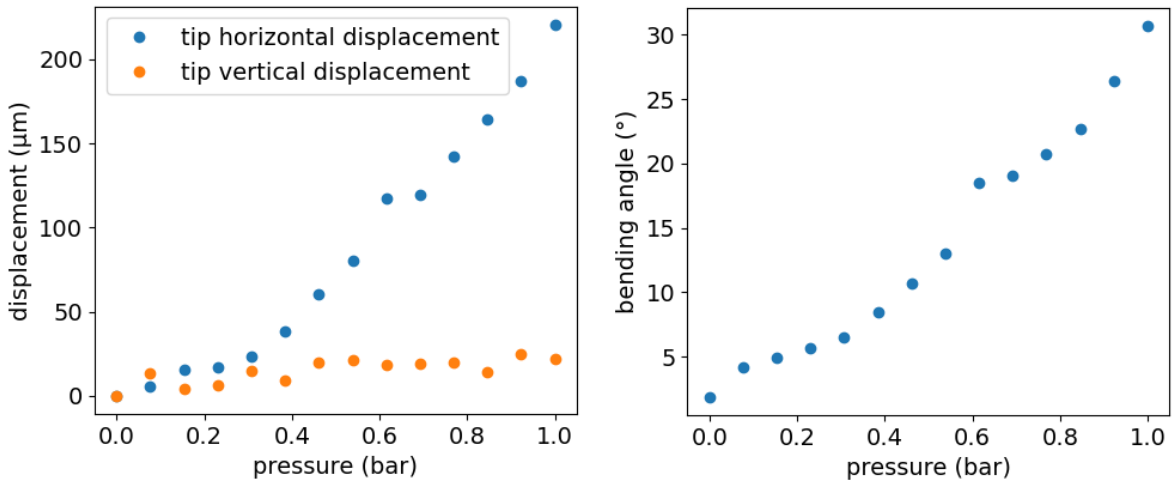

Figure S5. Characterization of the microactuator (R=150, r=90, e=42 µm) inflation. Tip displacements (left panel) and bending angle (right panel) are obtained though image analysis from the optical microscopy.